
Wi-CBR: WiFi-based Cross-domain Behavior Recognition via Multimodal Collaborative Awareness

Ruobei Zhang, Shengeng Tang*, Huan Yan, Xiang Zhang, Richang Hong
 Hefei University of Technology
 zrb@mail.hfut.edu.cn, tangsg@hfut.edu.cn

Abstract

WiFi-based human behavior recognition aims to recognize gestures and activities by analyzing wireless signal variations. However, existing methods typically focus on a single type of data, neglecting the interaction and fusion of multiple features. To this end, we propose a novel multimodal collaborative awareness method. By leveraging phase data reflecting changes in dynamic path length and Doppler Shift (DFS) data corresponding to frequency changes related to the speed of gesture movement, we enable efficient interaction and fusion of these features to improve recognition accuracy. Specifically, we first introduce a dual-branch self-attention module to capture spatial-temporal cues within each modality. Then, a group attention mechanism is applied to the concatenated phase and DFS features to mine key group features critical for behavior recognition. Through a gating mechanism, the combined features are further divided into PD-strengthen and PD-weaken branches, optimizing information entropy and promoting cross-modal collaborative awareness. Extensive in-domain and cross-domain experiments on two large publicly available datasets, Widar3.0 and XRF55, demonstrate the superior performance of our method.

1 Introduction

Human Behavior Recognition (HBR) plays a crucial role in applications such as smart surveillance, healthcare, smart homes, and human-computer interaction. HBR can be classified into sensor-based, vision-based, and wireless signal-based [1, 2, 3] approaches. With the widespread deployment of WiFi systems and advancements in wireless technology, HBR using wireless sensing has gained significant attention. HBR scenarios span indoor environments like homes, workplaces, and medical facilities, while behavior types include human-object, human-human, and human-computer interaction. Coarse-grained activities can be easily detected using motion tracking techniques, but fine-grained gestures, which involve subtle movements and minimal signal disruption, remain challenging to recognize [4].

WiFi signals, characterized by Channel State Information (CSI) or Received Signal Strength Indicator (RSSI), are used to model the wireless channel. The core idea of WiFi sensing is that the changes in CSI patterns due to human or object motion contain unique information. Gesture recognition, for example, is achieved by learning the mapping between these signal variations and human behaviors [5, 6]. CSI-based gesture recognition for cross-domain tasks can be broadly categorized into modeling-based and learning-based approaches.

Modeling-Based HBR. Model-based approaches primarily focus on developing signal processing algorithms to extract environment-independent features from received signals, such as Body Coordinate Velocity Profile (BVP) [7], Motion Change Pattern (MCP) [8], and Doppler Frequency Shift

*Corresponding author.

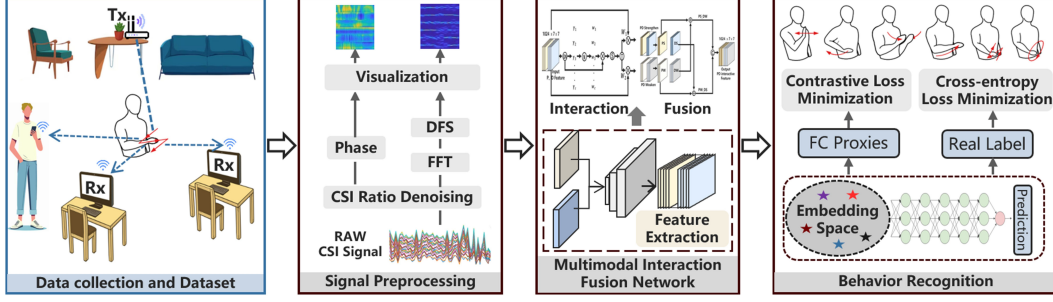


Figure 1: Wi-CBR Processing Flow.

(DFS) [9]. However, these methods have limitations, particularly in complex gesture recognition tasks, due to their inability to capture the full range of original data, which leads to reduced performance.

Learning-Based HBR. Recent advancements in deep learning have revolutionized various fields [10, 11], including Wi-Fi sensing. However, CSI signals present a significant challenge for learning-based approaches due to their sensitivity to environmental factors, such as the user’s location, orientation, and the surrounding environment. The received CSI signals not only encode information about the target object but also capture environment-specific details, such as static paths and noise, that are unrelated to the object being sensed [12, 13]. In cross-domain recognition, where the distribution of training and test data differs, this environmental noise complicates the task, necessitating the use of domain-invariant features to guide the learning process.

Due to the inherent limitations of the above approaches, we propose Wi-CBR to leverage the full spectrum of raw data while ensuring the integration of domain-independent features Fig 1. Specifically, our method introduces a novel multimodal collaborative awareness framework that efficiently combines phase data, which captures dynamic path length changes, and Doppler Shift (DFS) data, which reflects frequency shifts tied to gesture speed. To capture spatial-temporal patterns within each modality, we employ a dual-branch self-attention module, enabling the system to focus on important temporal and spatial features within each signal type. A group attention mechanism is then applied to the concatenated phase and DFS features, allowing the model to identify key group features that are essential for behavior recognition. Finally, a gating mechanism is used to divide the fused features into enhancement and suppression branches, optimizing information entropy and facilitating cross-modal collaborative complementarity. This fusion of multiple data sources, along with the innovative use of attention and gating mechanisms, enables more accurate and robust behavior recognition, particularly in cross-domain scenarios. Our main contributions are summarized as follows:

- We propose a multimodal collaborative awareness method for WiFi-based behavior recognition, which exploits two modal cues: phase and DFS. Phase reflects dynamic path length changes, while DFS captures the frequency variations related to gesture movement speed.
- A two-branch self-attention learning module is developed to capture the spatiotemporal cues within the modality, and a group attention mechanism is designed to mine key group features from the concatenated phase and DFS data.
- Through a gating mechanism, combined features are divided into PD-strengthen and PD-weaken branches, and collaborative awareness interactions are further performed to improve cross-modal complementarity.

2 Related Work

WiFi-based human behavior recognition [14, 15] can be broadly classified into modeling-based and learning-based approaches. Model-based methods rely on specialized knowledge to extract context-independent features from the original signal, but this can lead to the loss of important information. On the other hand, learning-based methods use machine learning for gesture recognition, though they often lack domain-independent feature guidance, limiting their effectiveness.

2.1 Modeling-Based HBR

Modeling-based approaches involve preprocessing raw CSI data, extracting manual features (e.g., velocity distribution statistics), and using machine learning models for gesture recognition [6, 16, 17, 18, 19, 20, 21, 22].

WiFinger [6] uses detailed CSI to recognize sign language, mitigating environmental noise and adapting to gesture inconsistency. Gao et al. [18] modeled the relationship between gesture signals and noise, using a dynamic phase exponential error (edp exponent) for gesture quality. Wi-NN [22] applies time-domain feature selection and a KNN classifier for recognition. WiGest [5] uses manually constructed patterns, but its reliance on coarse-grained RSS limits accuracy. WiMU [23] faces scalability issues due to manual pattern definitions, while WiDraw [24] requires over 25 WiFi transceivers for accurate hand tracking, making it impractical. QGesture [25] recognizes gestures with two antennas, but requires prior knowledge of hand position.

While these studies establish a correlation between WiFi signals and gestures, they overlook the impact of different environments on gesture recognition. Performing the same gesture in different environments can significantly alter WiFi waveforms [26, 27]. WiDar3 [7] introduces a domain-agnostic feature, BVP, unaffected by environmental factors, while WiHF [8] derives domain-independent motion patterns for cross-domain recognition. However, handcrafted features limit full spatiotemporal cue capture. WiGesture [28] shifts focus to hand-oriented features, extracting Motion Navigation Primitives (MNP) independent of position.

2.2 Learning-Based HBR

Learning-based methods rely on directly learning raw CSI data, such as amplitude and phase, for automatic pattern recognition.

Wikey [29] applies WiFi sensing for keystroke recognition, but it is highly sensitive to environmental changes. WiSign [30] extracts spatio-temporal features of amplitude and phase for continuous sign language recognition, but deep learning-based approaches require extensive domain-specific training. Tong et al. [31] developed a CSI-based gesture recognition system using a dynamic CNN-GRU-Attention (CGA) model and introduced techniques like phase correction and adaptive gesture action truncation to enhance data validity. Yang et al. [32] proposed a deep concatenated representation learning architecture combining CNNs and bidirectional RNNs for one-time gesture recognition, improving spatiotemporal pattern learning. WiHGR [33] builds a phase difference matrix and uses an improved Attention-Based Bidirectional Gate Recurrent Unit (ABGRU) to automatically extract discriminative features.

To address cross-domain challenges, some learning-based methods have also emerged. ABLSTM [34] introduced an attention-based framework that avoids the loss of implicit knowledge caused by handcrafted features. CROSSGR [35] extracts user-independent, gesture-related features from WiFi channel data, enhancing the system's utility without prior knowledge of the user. WiGr [36] utilizes query sample and class prototype similarity for gesture classification, mitigating cross-domain CSI variations. WIGRUNT [37] proposed a spatio-temporal dual-attention network that processes phase data into images for feature extraction using ResNet. Wi-SFDAGR [38] is the most recent work that tackles the cross-domain problem using Unsupervised Domain Adaptation (UDA), addressing scenarios where source data is unavailable during adaptation to unlabeled test data.

3 Method

Wi-CBR is divided into four main parts: signal preprocessing, two-branch intra-modal self-attention learning, cross-modal collaborative interaction fusion, and classification prediction. In signal preprocessing, the CSI-ratio model is used for denoising, and the DFS is obtained using STFT. Subsequently, the phase and DFS matrices of the CSI ratios are visualized as images suitable for deep learning processing. In the network part, initial feature extraction is achieved

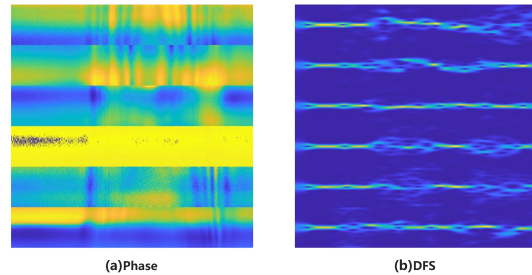


Figure 2: Phase and DFS visualization.

by two-branch intra-modal self-attentive learning as well as pre-trained ResNet18. Then, the feature fusion is achieved by a cross-model interactive fusion module. Finally, the behavior prediction is achieved by a classifier, and the two kinds of losses achieve constraints. As shown in Fig 3.

3.1 Task Definition

WiFi CSI describes the signal's attenuation on its propagation paths, such as scattering, multipath fading or shadowing, and power decay over distance. It can be characterized as:

$$\mathbf{Y} = \mathbf{H} \cdot \mathbf{X} + \mathbf{N}, \quad (1)$$

where \mathbf{Y} and \mathbf{X} are the received and transmitted signal vectors, respectively. \mathbf{N} is the additive white Gaussian noise, and \mathbf{H} is the channel matrix representing CSI. CSI is a superposition of signals of all the propagation paths, and its channel frequency response (CFR) can be represented as:

$$H(f, t) = \sum_{m \in \Phi} a_m(f, t) e^{-j2\pi \frac{d_m(t)}{\lambda}}, \quad (2)$$

where f and t represent center frequency and time stamp, m is the multipath component. $a_m(f, t)$ and $d_m(t)$ denote the complex attenuation and propagation length of the m th multipath component, respectively. Φ denotes the set of multipath components, and λ is the signal wavelength. In the case of CSI-based gesture recognition, the multipath component m consists of dynamic and static paths:

$$H(f, t) = H_s(f, t) + H_d(f, t) = \sum_{m_s \in \Phi_s} a_{m_s}(f, t) e^{-j2\pi \frac{d_{m_s}(t)}{\lambda}} + \sum_{m_d \in \Phi_d} a_{m_d}(f, t) e^{-j2\pi \frac{d_{m_d}(t)}{\lambda}}. \quad (3)$$

3.2 CSI Denoising Preprocessing

As demonstrated in the previous section, the gesture can be portrayed by the change of phase-shift in CSI. Unfortunately, for commodity WiFi devices, as the transmitter and receiver are not synchronized, there exists a time-varying random phase offset $e^{-j\theta_{\text{offset}}}$:

$$H(f, t) = e^{-j\theta_{\text{offset}}} (H_s(f, t) + H_d(f, t)) = e^{-j\theta_{\text{offset}}} \left(H_s(f, t) + A(f, t) e^{-j2\pi \frac{d(t)}{\lambda}} \right), \quad (4)$$

where $A(f, t)$, $e^{-j2\pi \frac{d(t)}{\lambda}}$, and $d(t)$ denote the complex attenuation, phase-shift, and path length of dynamic components, respectively. This random offset thus prevents us from directly using the CSI phase information.

Therefore, we need to eliminate $e^{-j\theta_{\text{offset}}}$. Fortunately, for commodity WiFi cards, this random offset remains the same across different antennas on the same WiFi network interface card (NIC) as they share the same RF oscillator. Thus, it can be eliminated by the CSI-ratio model [16, 25]:

$$H_r(f, t) = \frac{H_1(f, t)}{H_2(f, t)} = \frac{e^{-j\theta_{\text{offset}}} (H_{s,1} + H_{d,1})}{e^{-j\theta_{\text{offset}}} (H_{s,2} + H_{d,2})} = \frac{A_1 e^{-j2\pi \frac{d_1(t)}{\lambda}} + H_{s,1}}{A_2 e^{-j2\pi \frac{d_1(t) + \Delta d}{\lambda}} + H_{s,2}}, \quad (5)$$

where $H_1(f, t)$ and $H_2(f, t)$ are the CSI of two receiving antennas. When two antennas are close to each other, Δd can be regarded as a constant. According to Mobius transformation [39], (5) represents transformations such as scaling and rotation of the phase-shift $e^{-j2\pi \frac{d_1(t)}{\lambda}}$ of antenna 1 in the complex plane, and these transformations will not affect the changing trend of the phase-shift [40, 41, 42].

CSI to Phase. Phase P extracted from H_r can be used to describe gestures:

$$Phase = \text{angle}(H_r), \quad (6)$$

where $\text{angle}(\cdot)$ denotes the phase extraction function. For a complex $z = \text{abs}(z) \cdot e^{j\theta}$, we can use $\text{angle}(\cdot)$ to obtain the phase of z , $\theta = \text{angle}(z)$. The visualized Phase image is shown in Fig. 2(a).

CSI to DFS. The DFS captures frequency changes due to gesture motion, such as hand speed. To extract DFS, the **Short-Time Fourier Transform** is applied to $H_q(f, t)$:

$$S_f(\tau, \omega) = \int_{-\infty}^{\infty} H_q(f, t) w(t - \tau) e^{-j\omega t} dt, \quad (7)$$

where: $w(t - \tau)$: Window function (e.g., Hanning window) to segment the signal. τ : Time localization. ω : Frequency in radians, tied to the Doppler shift. The **power spectrogram** is then computed:

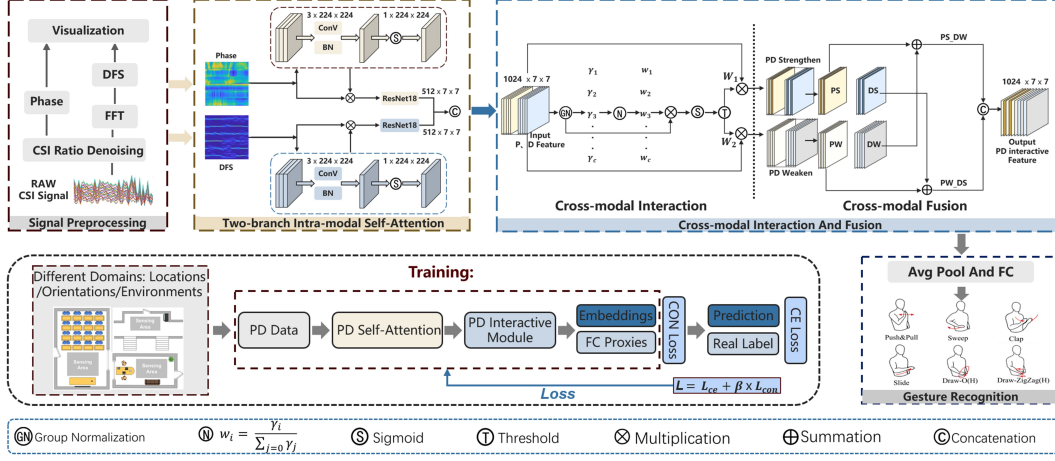


Figure 3: The System framework of Wi-CBR. Wi-CBR is divided into four main parts: Signal Pre-processing, Two-branch Intra-modal Self-attention Learning, Cross-modal Collaborative Interaction Fusion, and Gesture Recognition.

$$\text{DFS} = |S_f(\tau, \omega)|^2 = \left| \int_{-\infty}^{\infty} H_q(f, t) w(t - \tau) e^{-j\omega t} dt \right|^2. \quad (8)$$

In this spectrogram: The frequency ω at each time τ corresponds to the Doppler shift $f_d = \frac{\omega}{2\pi} \cdot f_d$ is proportional to the gesture speed $v(t)$. Positive frequencies indicate motion toward the receiver, while negative frequencies indicate motion away. This time-frequency representation enables detailed analysis of gesture dynamics. For the Widar3.0 dataset, each DFS file is a $6 \times 121 \times T$ matrix, where the first dimension represents the 6 receivers, the second dimension represents the 121 frequency segments ranging from $[-60, 60]$ Hz, and the third dimension represents the timestamps with a sampling rate of 1000Hz. The visualized DFS image is shown in Fig. 2(b).

3.3 Two-branch Intra-modal Self-attention Learning

Two-Branch Self-attention. The proposed dual-path spatial attention mechanism processes phase (\mathbf{P}_x) and Doppler (\mathbf{D}_x) features through independent attention branches. Let $f_{\text{conv}}^{(k)}$ denote a convolution operation with kernel size $k \times k$, and BN represent batch normalization. The attention weights are computed as:

$$\mathbf{A}_p = \sigma \left(\text{BN} \left(f_{\text{conv}}^{(7)} \left(f_{\text{conv}}^{(7)} (\mathbf{P}_x) \right) \right) \right); \quad \mathbf{A}_d = \sigma \left(\text{BN} \left(f_{\text{conv}}^{(7)} \left(f_{\text{conv}}^{(7)} (\mathbf{D}_x) \right) \right) \right), \quad (9)$$

where $\sigma(\cdot)$ is the sigmoid function. The refined features are obtained through:

$$\mathbf{P}_{\text{out}} = \mathbf{P}_x \otimes \mathbf{A}_p \oplus \mathbf{P}_x; \quad \mathbf{D}_{\text{out}} = \mathbf{D}_x \otimes \mathbf{A}_d \oplus \mathbf{D}_x, \quad (10)$$

where \otimes is element-wise multiplication, \oplus is element-wise summation. Each branch maintains independent convolution parameters, with channel dimensions preserved in first convolution ($3 \rightarrow 3$) and reduced to single channel ($3 \rightarrow 1$) in the second convolution.

Two-Branch Feature Extraction. Independent spatial attention parameters for P/D branches; Separate batch normalization statistics for each modality; Symmetric padding (3 pixels) maintained in all convolutions; No parameter sharing between ϕ_{ResNet}^P and ϕ_{ResNet}^D .

$$\mathbf{X}_P = \phi_{\text{ResNet}}^P(\mathbf{P}_{\text{out}}); \quad \mathbf{X}_D = \phi_{\text{ResNet}}^D(\mathbf{D}_{\text{out}}), \quad (11)$$

where ϕ_{ResNet}^P and ϕ_{ResNet}^D denote independent ResNet-18 backbones. The final representation combines features through:

$$\mathbf{X}_{\text{PD}} = \text{Concat}(\mathbf{X}_P, \mathbf{X}_D) \in \mathbb{R}^{1024 \times 7 \times 7}. \quad (12)$$

3.4 Cross-modal Synergistic Interaction and Fusion

Cross-modal Interaction. To make the extracted Phase and DFS features interact and merge, we use group normalization to achieve the attention of different channels. The generated attention maps are thresholded to get the strengthened and weakened maps, and then the strengthened and weakened Phase and DFS features are obtained. Based on retaining important features and attenuating minor features [43], the feature space redundancy is reduced while utilizing both features.

Separate operation aims to separate those informative feature maps from less informative ones corresponding to the spatial content. We leverage the scaling factors in Group Normalization (GN) [44] layers to assess the informative content of different feature maps. To be concrete, given an intermediate feature map $X_{PD} \in \mathbb{R}^{N \times C \times H \times W}$, where N is the batch axis, C is the channel axis, H and W are the spatial height and width axes. We first standardize the input feature X by subtracting mean μ and dividing by standard deviation σ as follows:

$$X_{gn} = \text{GN}(X_{PD}) = \gamma \frac{X_{PD} - \mu}{\sqrt{\sigma^2 + \epsilon}} + \beta, \quad (13)$$

where μ and σ are the mean and standard deviation of X_{PD} , ϵ is a small positive constant added for numerical stability, γ and β are trainable affine transformation parameters.

Noted that we leverage the trainable parameters $\gamma \in \mathbb{R}^C$ in GN layers as a way to measure the variance of spatial pixels for phase and DFS. The richer spatial information reflects more variation in spatial pixels contributing to a larger γ . The normalized correlation weights $W_\gamma \in \mathbb{R}^C$ are obtained by equation 14, which indicates the importance of different phase and DFS feature maps.

$$W_\gamma = \{w_i\} = \frac{\gamma_i}{\sum_{j=1}^C \gamma_j}, \quad i, j = 1, 2, \dots, C. \quad (14)$$

Then the weight values of feature maps reweighted by W_γ are mapped to the range (0, 1) by the sigmoid function and gated by a threshold. We set those weights above the threshold to 1 to obtain the informative weights W_1 while setting them to 0 to gain the non-informative weights W_2 (the threshold is set to 0.5 in the experiments). The whole process of acquiring W can be expressed as equation (16):

$$W = \text{Gate}(\text{Sigmoid}(W_\gamma(\text{GN}(X_{PD}))))). \quad (15)$$

We multiply input features X_{PD} by W_1 and W_2 respectively, yielding two weighted features: the strengthen ones X_{PD}^S and less informative ones X_{PD}^W . Thus, we completed the interaction between the input phase and DFS features. The attention weights are obtained by learning the variance and bias through group normalization, which is gated to obtain the strengthened and weakened attention maps. Two components obtained are as follows: X_{PD}^S has informative and expressive spatial content and is strengthened, while X_{PD}^W has little or no information, which is considered redundant and weakened.

Cross-modal Fusion. We propose a fusion operation to achieve synergistic utilization. An information-rich feature after strengthening is added to a feature with less information after weakening. New features with richer information are generated, i.e., one feature dominates while the other aids. Instead of adding the two components directly, we use a cross-fertilization operation to thoroughly combine the two weighted different information features to enhance the information flow between them. The cross-rendered features X_{w1} and X_{w2} are then stitched together to obtain a spatially fine feature mapping of X_w . The whole process of Fusion operation can be expressed as :

$$\begin{cases} X_{PD}^S = W_1 \otimes X_{PD}, X_{PD}^W = W_2 \otimes X_{PD}; \\ Y_{PS_DW} = X_P^S \oplus X_D^W, Y_{PW_DS} = X_P^W \oplus X_D^S; \\ X_{out} = Y_{PS_DW} \cup Y_{PW_DS}, \end{cases} \quad (16)$$

where \otimes is element-wise multiplication, \oplus is element-wise summation, \cup is concatenation. Y_{PS_DW} is a phase-dominant DFS-assisted fusion feature, while Y_{PW_DS} is a phase-assisted DFS-dominant fusion feature. After the Cross-Model Fusion is applied to the intermediate input features X_{PD} , not only do we separate the informative features from less informative ones, but also we reconstruct them to enhance the representative features and suppress the redundant features in spatial dimension.

3.5 Gestrue Recognition and Contrastive Loss Optimization

Building upon the aforementioned modules, we obtain the Cross-Model Fusion feature representation X_{out} . Most existing works directly feed the global representation X_{out} into the classifier (i.e., a fully-connected layer with a Softmax) to predict the probability of gestures \hat{y} . The model is then trained by minimizing the corresponding loss L_{ce} between the prediction values \hat{y} and their ground truths y .

$$\hat{y} = f_{\text{classifier}}(X_{\text{out}}; \Theta_{\text{classifier}}), \quad (17)$$

$$\mathcal{L}_{ce} = \mathcal{L}_{ce}(y, \hat{y}) = \frac{1}{M} \sum_{m=1}^M \sum_{s=1}^S y_{m,s} \log(\hat{y}_{m,s}), \quad (18)$$

where $\Theta_{\text{classifier}}$ is the learned parameter, L_{ce} is a classification cross-entropy loss, and M is the number of data samples, S is the number of gestures.

Contrastive Loss optimizes the objective by learning a distance measure based on multiple positive and negative sample-to-sample pairs. The key idea behind this is to learn an embedding space where similar pairs of samples are close to each other and dissimilar pairs are far apart. Thus, we can obtain an invariant representation across different environments for the same instance, i.e., a domain-independent characterization. We aim to learn generalizable representations by minimizing the following contrast-based objective. For the i th sample extracted feature x_i :

$$\mathcal{L}_{con} = -\frac{1}{N} \sum_{i=1}^N \log \frac{e^{(x_i^T x_+)/\tau}}{e^{(x_i^T x_+)/\tau} + \sum e^{(x_i^T x_-)/\tau}}, \quad (19)$$

where, the pair (x_i, x_+) represents samples of the same class (positive pair), while (x_i, x_-) denotes samples from different classes (negative pair), with τ serving as the temperature parameter. Several elements can influence the variation patterns of the CSI signal, with varying degrees of effect. For example, a user's influence on signal patterns is less significant compared to changes in location and orientation. Importantly, positive sample pairs across diverse environments differ, and some may be challenging to match due to substantial data discrepancies. Perfectly aligning all negative samples might limit the model's ability to generalize. To mitigate this, we utilize class proxies to symbolize each gesture, ideally enhancing resilience across samples from varied settings. Formally, these proxy vectors are defined as the weights of the final fully connected layer in the classifier. To further improve semantic consistency, we implement a proxy-based contrastive loss that utilizes the connections between class proxies and samples to foster robust representations [45]. Given the representation x_i of i th sample, we select its class proxy w_c in place of positive samples x_+ to form proxy-to-sample positive pairs. The contrast loss is incorporated into the overall loss function \mathcal{L} :

$$\mathcal{L}_{con} = -\frac{1}{N} \sum_{i=1}^N \log \frac{e^{(w_c^T x_i)/\tau}}{e^{(w_c^T x_i)/\tau} + \sum_{k=1, k \neq c}^R e^{(w_k^T x_i)/\tau}}; \quad \mathcal{L} = \mathcal{L}_{ce} + \mathcal{L}_{con}, \quad (20)$$

where w_c represents the class proxy of sample i , R is the number of classes, and P is the number of negative pairs. In general, we aim to minimize the following final loss function, where \mathcal{L}_{ce} is cross-entropy loss, and \mathcal{L}_{con} is the proxy-based contrastive loss. β is trade-off parameter.

4 Experiments

4.1 Implementation Details

Datasets Setting. To evaluate the effectiveness of our model for cross-domain gesture recognition, we conducted extensive experiments on the Widar 3.0 and XRF55 datasets. For in-domain, cross-location, and orientation evaluations on Widar 3.0, we used 80% of the data for training and 20% for testing with five-fold cross-validation. For cross-location evaluation, one location was used for testing and the remaining four for training. The in-domain and cross-direction evaluations followed a similar approach. For cross-environment evaluation, we used data from three environments, totaling 12,750 samples (17 users \times 5 locations \times 5 directions \times 6 gestures \times 5 instances), with training on two environments and testing on the third using triple cross-validation. For XRF55, the cross-environment evaluation involved four scenarios, with quad-fold cross-validation on 6,240 samples.

In our implementation, we used Matlab to preprocess CSI data and generate 224 \times 224 RGB images. After obtaining phase and DFS images, all models were implemented in PyTorch 1.13.1. The network

Table 1: THE accuracy of Wi-CBR under CL(Cross-location), CO(Cross-orientation), and CE(Cross-environment) settings in the WIDAR3.0 dataset and the XRF55 dataset.

Method	Processing Flow	Widar3.0			Mean	XRF55
		CL	CO	CE		
Widar3.0 [7]	CSI→DFS→BVP	90.48%	81.58%	83.30%	85.12%	–
ImgFi [48]	CSI→STFT, RT image	39.58%	38.12%	40.37%	39.36%	31.90%
EI [49]	CSI→amplitude	73.33%	79.70%	–	–	–
WiSR [50]	CSI image	67.73%	69.74%	52.77%	63.41%	26.66%
Recurrent ConFormer [51]	Raw CSI	73.84%	85.88%	50.38%	70.03%	16.54%
THAT [52]	Raw CSI	71.56%	81.76%	49.71%	67.68%	23.23%
WiHF [8]	CSI→DFS→MCP	91.22%	80.64%	–	–	–
WIGNN [53]	CSI→DFS	95.20%	93.30%	–	–	–
WIGRUNT [37]	CSI→Phase	97.08%	93.39%	95.36%	95.28%	55.92%
WiDual [54]	CSI→Phase	97.39%	94.87%	–	–	–
AaD [55]	CSI→Phase	95.90%	95.38%	93.00%	94.83%	55.64%
Wi-SFDAGR [38]	CSI→Phase	97.30%	97.17%	95.52%	96.66%	57.99%
Wi-CBR	CSI→Phase, DFS	98.34%	96.30%	96.57%	97.07%	66.05%

architecture and data dimensions are shown in Fig. 3. Wi-CBR employs ResNet-18 [46] with pre-trained ImageNet weights as the feature extractor, addressing parameter learning challenges due to limited training data [37, 47]. The Cross-Model Interaction module uses 4 groups, with a threshold set at 0.5. The contrast loss weight β and temperature are both set to 0.1. During training, the model is optimized using Adam with a learning rate of 0.001, a batch size of 10, and 30 epochs. We used the same network structure for both the Widar 3.0 and XRF55 datasets, ensuring robustness across datasets. The final fully connected layer is adjusted to 6 or 8 units, corresponding to the number of gestures in each dataset. A random seed of 42 was set for reproducibility.

4.2 Overall Performance

Comparison with state-of-the-art methods. We first evaluate the overall performance of Wi-CBR in cross-location, cross-orientation, and cross-environment scenarios, compared with some cross-domain recognition methods, as shown in Tab. 1. **Modeling-Based method:** Widar3.0 [7], WiHF [8], WIGNN [53]. They extract DFS features from denoised CSI data, and some further manually extract domain-independent features such as BVP and MCP. The cross-domain average performance of these methods on the Widar3.0 dataset can reach 85.12%. **Low Level Semantic Learning-Based method:** ImgFi [48], EI [49], WiSR [50], Recurrent ConFormer [51], THAT [52]. They use low-level semantic data, such as raw CSI, amplitude, and preliminary CSI visualization images, which can be found. The average cross-domain performance of these efforts on the Widar 3.0 dataset ranges from 40% to 70%, while switching to the XRF55 dataset, the maximum is only up to 31.90%. **High Level Semantic Learning-Based method:** WIGRUNT [37], WiDual [54], AaD [55], Wi-SFDAGR [38]. They use CSI-ratio for the denoising extraction phase and then use an efficient ResNet18 backbone network as a feature extractor. In particular, Wi-SFDAGR uses attraction-dispersion networks to optimize prediction boundaries and enhance feature aggregation. The cross-domain average performance reaches 96.66% on Widar 3.0.

Wi-CBR generally outperforms state-of-the-art work on both datasets. In addition, we observe an interesting phenomenon: The performance across environments on the XRF55 dataset is lower than that of Widar3.0, regardless of which method is used. This is because the XRF55 dataset has a lower sampling rate than Widar3.0,

and the number of receiver arrangements in the environment is half that of Widar3.0. Wi-CBR, on the other hand, demonstrates robustness across datasets, and our work still achieves 66.05% accuracy despite changes in conditions such as receiver and sampling rate.

Table 2: Detailed performance on Widar 3.0 and XRF55.

Dataset	Setting	1	2	3	4	5
Widar 3.0	In-Domain	99.04%	99.70%	99.48%	99.78%	99.70%
	CL	97.85%	97.63%	98.74%	98.00%	99.48%
	CO	92.07%	98.22%	97.85%	99.19%	94.15%
	CE	93.19%	99.33%	97.20%	–	–
XRF55	CE	55.65%	68.13%	72.50%	67.92%	–

For the Widar 3.0 dataset, Wi-CBR has an average recognition accuracy of 99.54% for in-domain gesture recognition and 98.34%, 96.30%, and 96.57% for cross-location, orientation, and environment, respectively. For the XRF55 dataset, the average recognition accuracy across environments is 66.05%. The detailed results are shown in Tab. 2. The Setting denotes the data for testing while others for training. To analyze recognition accuracy and misclassifica-

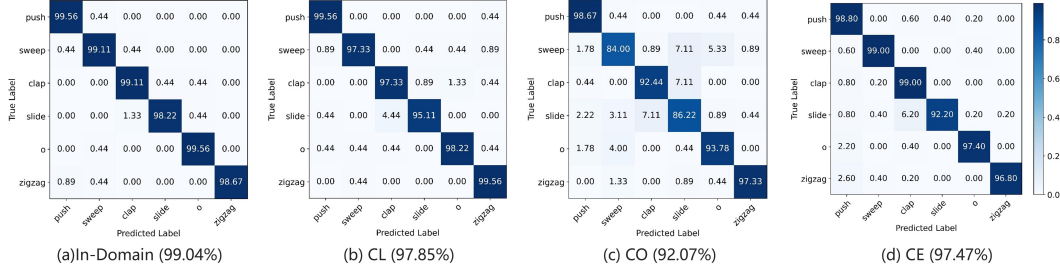


Figure 4: The confusion matrices of our method in the indomain (repetition 1), CL (location 1), CO (orientation 1), and CE (environment 3) settings.

tion rates, we present confusion matrices for test location 1, orientation 1, and environment 3 on Widar 3.0, as shown in Fig. 4. In cross-location and cross-orientation tests, “push” and “zigzag” gestures achieve the highest accuracy, while “slide” and “sweep” show the lowest, respectively. In the cross-environment test, “sweep” and “clap” perform best. Interestingly, “slide” is frequently misclassified as “clap.” This likely stems from similar motion trajectories, as both gestures involve inclined or sliding movements, making them harder to distinguish.

Ablation Study. We evaluate four variants of our model to conduct an ablation study. Wi-CBR w/o D: Only the CSI ratio phase is used as input data for the model. Wi-CBR w/o P: Only the DFS image is utilized as input data. Wi-CBR w/o IF: No interaction, use WiGRUNT [37] channel-attention module CRU instead of ours. Wi-CBR w/o CL: Only use cross-entropy loss.

Table 3: Ablation Analysis in Different Settings

Methods	In-Domain	CL	CO	CE
Wi-CBR	99.54%	98.34%	96.30%	96.57%
Wi-CBR w/o D	99.42%	96.07%	92.76%	93.76%
Wi-CBR w/o P	97.13%	95.04%	87.09%	94.93%
Wi-CBR w/o IF	99.11%	97.07%	95.07%	95.93%
Wi-CBR w/o CL	99.49%	97.26%	95.56%	96.08%

The results in Tab. 3 show that input data significantly affects model performance, with phase data and DFS both contributing to recognition accuracy. Phase data provides comprehensive raw information, while DFS has some omissions. Removing our feature interaction and fusion modules consistently reduced model accuracy, highlighting the importance of cross-modal interaction for balancing phase and DFS data. The multimodal fusion module effectively integrates different modal features. Additionally, omitting contrast loss guidance led to a noticeable drop in cross-domain performance, while intra-domain performance remained stable, indicating that contrast loss helps the model focus on gesture-related features rather than environmental noise. Overall, Wi-CBR effectively leverages full CSI raw data and DFS for improved cross-domain performance.

5 Conclusion

We propose Wi-CBR, a WiFi-based cross-domain human behavior recognition framework with strong cross-domain performance. It combines model-based and learning-based approaches, leveraging phase data (dynamic path length changes) and DFS data (frequency changes related to gesture speed). By utilizing full data and domain-independent feature guidance, Wi-CBR enhances recognition accuracy. The framework includes a two-branch self-attention module to capture spatio-temporal cues, followed by bi-gating for feature enhancement and suppression. Cross-modal data fusion in both time and frequency domains enables robust behavioral feature extraction, focusing on the behavior itself while minimizing environmental influence.

References

- [1] Z. Sun, Q. Ke, H. Rahmani, M. Bennamoun, G. Wang, and J. Liu. Human action recognition from various data modalities: A review. *IEEE Transactions on Pattern Analysis and Machine Intelligence*, 45(3):3200–3225, 2022.
- [2] Y. Wang, S. Cang, and H. Yu. A survey on wearable sensor modality centred human activity recognition in health care. *Expert Systems with Applications*, 137:167–190, 2019.
- [3] S. K. Yadav, K. Tiwari, H. M. Pandey, and S. A. Akbar. A review of multimodal human activity recognition with special emphasis on classification, applications, challenges and future directions. *Knowledge-Based Systems*, 223:106970, 2021.
- [4] M. C. Corballis. The gestural origins of language. *Wiley Interdisciplinary Reviews: Cognitive Science*, 1(1):2–7, 2010.
- [5] Heba Abdelnasser, Moustafa Youssef, and Khaled A Harras. Wigest: A ubiquitous wifi-based gesture recognition system. In *2015 IEEE Conference on Computer Communications (INFOCOM)*, pages 1472–1480. IEEE, 2015.
- [6] Sheng Tan and Jie Yang. Wifinger: Leveraging commodity wifi for fine-grained finger gesture recognition. In *Proceedings of the 17th ACM International Symposium on Mobile Ad Hoc Networking and Computing*, pages 201–210, 2016.
- [7] Y. Zheng, Y. Zhang, K. Qian, G. Zhang, Y. Liu, C. Wu, and Z. Yang. Zero-effort cross-domain gesture recognition with wi-fi. In *Proceedings of the 17th annual international conference on mobile systems, applications, and services*, pages 313–325, 2019.
- [8] C. Li, M. Liu, and Z. Cao. Wihf: Enable user identified gesture recognition with wifi. In *IEEE INFOCOM 2020-IEEE Conference on Computer Communications*, pages 586–595, 2020.
- [9] K. Niu, F. Zhang, X. Wang, Q. Lv, H. Luo, and D. Zhang. Understanding wifi signal frequency features for position-independent gesture sensing. *IEEE Transactions on Mobile Computing*, 21(11):4156–4171, 2021.
- [10] Jiuxiang Gu, Zhenhua Wang, Jason Kuen, Lianyang Ma, Amir Shahroudy, Bing Shuai, Ting Liu, Xingxing Wang, Gang Wang, Jianfei Cai, et al. Recent advances in convolutional neural networks. *Pattern Recognition*, 77:354–377, 2018.
- [11] Yann LeCun, Yoshua Bengio, and Geoffrey Hinton. Deep learning. *Nature*, 521(7553):436–444, 2015.
- [12] Dan Wu, Ruiyang Gao, Youwei Zeng, Jinyi Liu, Leye Wang, Tao Gu, and Daqing Zhang. Fingerdraw: Sub-wavelength level finger motion tracking with wifi signals. *Proceedings of the ACM on Interactive, Mobile, Wearable and Ubiquitous Technologies*, 4(1):1–27, 2020.
- [13] Daqing Zhang, Hao Wang, and Dan Wu. Toward centimeter-scale human activity sensing with wi-fi signals. *Computer*, 50(1):48–57, 2017.
- [14] Q. Pu, S. Gupta, S. Gollakota, and S. Patel. Whole-home gesture recognition using wireless signals. In *Proceedings of the 19th Annual International Conference on Mobile Computing and Networking*, pages 27–38, 2013.
- [15] Y. Wang, J. Liu, Y. Chen, M. Gruteser, J. Yang, and H. Liu. E-eyes: Device-free location-oriented activity identification using fine-grained wifi signatures. In *Proceedings of the 20th Annual International Conference on Mobile Computing and Networking*, pages 617–628, 2014.
- [16] G. Tong, Y. Li, H. Zhang, and N. Xiong. A fine-grained channel state information-based deep learning system for dynamic gesture recognition. *Information Sciences*, 636:118912, 2023.
- [17] Y. Gu, H. Yan, X. Zhang, Y. Wang, J. Huang, Y. Ji, and F. Ren. Attention-based gesture recognition using commodity wifi devices. *IEEE Sensors Journal*, 23(9):9685–9696, 2023.

- [18] R. Gao, W. Li, Y. Xie, E. Yi, L. Wang, D. Wu, and D. Zhang. Towards robust gesture recognition by characterizing the sensing quality of wifi signals. *Proceedings of the ACM on Interactive, Mobile, Wearable and Ubiquitous Technologies*, 6(1):1–26, 2022.
- [19] J. Yang, H. Zou, Y. Zhou, and L. Xie. Learning gestures from wifi: A siamese recurrent convolutional architecture. *IEEE Internet of Things Journal*, 6(6):10763–10772, 2019.
- [20] W. Meng, X. Chen, W. Cui, and J. Guo. Wihgr: A robust wifi-based human gesture recognition system via sparse recovery and modified attention-based bgru. *IEEE Internet of Things Journal*, 9(12):10272–10282, 2021.
- [21] S. D. Regani, B. Wang, and K. R. Liu. Wifi-based device-free gesture recognition through-the-wall. In *ICASSP 2021-2021 IEEE International Conference on Acoustics, Speech and Signal Processing (ICASSP)*, pages 8017–8021. IEEE, 2021.
- [22] Y. Zhang, B. Yuan, Z. Yang, Z. Li, and X. Liu. Wi-nn: Human gesture recognition system based on weighted knn. *Applied Sciences*, 13(6):3743, 2023.
- [23] R. H. Venkatnarayan, G. Page, and M. Shahzad. Multi-user gesture recognition using wifi. In *Proc. 16th Annu. Int. Conf. Mobile Syst., Appl., Serv.*, pages 401–413, 2018.
- [24] L. Sun, S. Sen, D. Koutsonikolas, and K.-H. Kim. Widraw: Enabling hands-free drawing in the air on commodity wifi devices. In *Proceedings of the 21st Annual International Conference on Mobile Computing and Networking*, pages 77–89, 2015.
- [25] N. Yu, W. Wang, A. X. Liu, and L. Kong. Qgesture: Quantifying gesture distance and direction with wifi signals. *ACM Interactive, Mobile, Wearable and Ubiquitous Technologies*, 2(1):1–23, 2018.
- [26] C. Chen, G. Zhou, and Y. Lin. Cross-domain wifi sensing with channel state information: A survey. *ACM Computing Surveys*, 55(11):1–37, 2023.
- [27] H. Kang, Q. Zhang, and Q. Huang. Context-aware wireless-based cross-domain gesture recognition. *IEEE Internet of Things Journal*, 8(17):13503–13515, 2021.
- [28] R. Gao, M. Zhang, J. Zhang, Y. Li, E. Yi, D. Wu, L. Wang, and D. Zhang. Towards position-independent sensing for gesture recognition with wifi. *Proceedings of the ACM on Interactive, Mobile, Wearable and Ubiquitous Technologies*, 5(2):1–28, 2021.
- [29] K. Ali, A. X. Liu, W. Wang, and M. Shahzad. Keystroke recognition using wifi signals. In *Proc. 21st Annu. Int. Conf. Mobile Comput. Netw.*, pages 90–102, 2015.
- [30] L. Zhang, Y. Zhang, and X. Zheng. Wisign: Ubiquitous american sign language recognition using commercial wi-fi devices. *ACM Trans. Intell. Syst. Technol.*, 11(3):1–24, 2020.
- [31] G. Tong, Y. Li, H. Zhang, and N. Xiong. A fine-grained channel state information-based deep learning system for dynamic gesture recognition. *Information Sciences*, 636:118912, 2023.
- [32] J. Yang, H. Zou, Y. Zhou, and L. Xie. Learning gestures from wifi: A siamese recurrent convolutional architecture. *IEEE Internet of Things Journal*, 6(6):10763–10772, 2019.
- [33] W. Meng, X. Chen, W. Cui, and J. Guo. Wihgr: A robust wifi-based human gesture recognition system via sparse recovery and modified attention-based bgru. *IEEE Internet of Things Journal*, 9(12):10272–10282, 2021.
- [34] Z. Chen, L. Zhang, C. Jiang, Z. Cao, and W. Cui. Wifi csi based passive human activity recognition using attention based blstm. *IEEE Transactions on Mobile Computing*, 18(11):2714–2724, Nov 2019.
- [35] X. Li, L. Chang, F. Song, J. Wang, X. Chen, Z. Tang, and Z. Wang. Crossgr: Accurate and low-cost cross-target gesture recognition using wi-fi. *Proceedings of the ACM on Interactive, Mobile, Wearable and Ubiquitous Technologies*, 5(1):1–23, 2021.
- [36] X. Zhang, C. Tang, K. Yin, and Q. Ni. Wifi-based cross-domain gesture recognition via modified prototypical networks. *IEEE Internet of Things Journal*, 9(11):8584–8596, 2021.

- [37] Y. Gu, X. Zhang, Y. Wang, M. Wang, H. Yan, Y. Ji, and M. Dong. Wigrunt: Wifi-enabled gesture recognition using dual-attention network. *IEEE Transactions on Human-Machine Systems*, 52(4):736–746, 2022.
- [38] H. Yan, X. Zhang, J. Huang, Y. Feng, M. Li, A. Wang, and Z. Liu. Wi-sfdagr: Wifi-based cross-domain gesture recognition via source-free domain adaptation. *IEEE Internet of Things Journal*, 2025.
- [39] Y. Zeng, D. Wu, J. Xiong, E. Yi, R. Gao, and D. Zhang. Farsense: Pushing the range limit of wifi-based respiration sensing with csi ratio of two antennas. *Proceedings of the ACM on Interactive, Mobile, Wearable and Ubiquitous Technologies*, 3(3):1–26, 2019.
- [40] M. Kotaru, K. Joshi, D. Bharadia, and S. Katti. Spotfi: Decimeter level localization using wifi. In *Proceedings of the ACM Conference on Special Interest Group on Data Communication (SIGCOMM)*, pages 269–282. ACM, 2015.
- [41] X. Li, S. Li, D. Zhang, J. Xiong, Y. Wang, and H. Mei. Dynamic-music: Accurate device-free indoor localization. In *Proceedings of the ACM International Joint Conference on Pervasive and Ubiquitous Computing (UbiComp)*, pages 196–207. ACM, 2016.
- [42] Y. Zeng, D. Wu, R. Gao, T. Gu, and D. Zhang. Fullbreathe: Full human respiration detection exploiting complementarity of csi phase and amplitude of wifi signals. *Proceedings of the ACM on Interactive, Mobile, Wearable and Ubiquitous Technologies (IMWUT)*, 2(3):1–19, 2018.
- [43] J. Li, Y. Wen, and L. He. Scconv: Spatial and channel reconstruction convolution for feature redundancy. In *Proceedings of the IEEE/CVF Conference on Computer Vision and Pattern Recognition*, pages 6153–6162. IEEE/CVF, 2023.
- [44] Y. Wu and K. He. Group normalization. In *Proceedings of the European Conference on Computer Vision (ECCV)*, pages 3–19. Springer, 2018.
- [45] X. Yao, Y. Bai, X. Zhang, Y. Zhang, Q. Sun, R. Chen, R. Li, and B. Yu. Pcl: Proxy-based contrastive learning for domain generalization. In *Proceedings of the IEEE/CVF Conference on Computer Vision and Pattern Recognition (CVPR)*, pages 7097–7107. IEEE/CVF, 2022.
- [46] K. He, X. Zhang, S. Ren, and J. Sun. Deep residual learning for image recognition. In *Proceedings of the IEEE Conference on Computer Vision and Pattern Recognition (CVPR)*, pages 770–778. IEEE, 2016.
- [47] X. Zheng, K. Yang, J. Xiong, L. Liu, and H. Ma. Pushing the limits of wifi sensing with low transmission rates. *IEEE Transactions on Mobile Computing*, 2024. Early Access.
- [48] C. Zhang and W. Jiao. Imgfi: A high accuracy and lightweight human activity recognition framework using csi image. *IEEE Sensors Journal*, 23(18):21966–21977, 2023.
- [49] W. Jiang, C. Miao, F. Ma, S. Yao, Y. Wang, Y. Yuan, and L. Su. Towards environment independent device free human activity recognition. In *Proceedings of the 24th annual international conference on mobile computing and networking*, pages 289–304, 2018.
- [50] S. Liu, Z. Chen, M. Wu, C. Liu, and L. Chen. Wisr: Wireless domain generalization based on style randomization. *IEEE Transactions on Mobile Computing*, 23(5):4520–4532, 2023.
- [51] M. Shang and X. Hong. Recurrent conformer for wifi activity recognition. *IEEE/CAA Journal of Automatica Sinica*, 10(6):1491–1493, 2023.
- [52] B. Li, W. Cui, W. Wang, L. Zhang, Z. Chen, and M. Wu. Two-stream convolution augmented transformer for human activity recognition. In *Proceedings of the AAAI conference on artificial intelligence*, volume 35, pages 286–293, 2021.
- [53] Y. Chen and X. Huang. Wignn: Wifi-based cross-domain gesture recognition inspired by dynamic topology structure. *IEEE Wireless Communications*, 31(3):249–256, 2024.
- [54] M. Dai, C. Cao, T. Liu, M. Su, Y. Li, and J. Li. Widual: User identified gesture recognition using commercial wifi. In *2023 IEEE/ACM 23rd International Symposium on Cluster, Cloud and Internet Computing (CCGrid)*, pages 673–683, 2023.

- [55] S. Yang, S. Jui, and J. Van De Weijer. Attracting and dispersing: A simple approach for source-free domain adaptation. *Advances in Neural Information Processing Systems*, 35:5802–5815, 2022.
- [56] F. Wang, Y. Lv, M. Zhu, H. Ding, and J. Han. Xrf55: A radio frequency dataset for human indoor action analysis. *Proceedings of the ACM on Interactive, Mobile, Wearable and Ubiquitous Technologies*, 8(1):1–34, 2024.

A More Implementation Details

Dataset Details.

Widar3.0 [7] is one of the most widely used datasets for WiFi-based gesture recognition. The dataset collection device consists of one transmitter and six receivers, each equipped with an Intel 5300 wireless card. Each receiver has three antennas arranged in a line. The operating frequency of the device is 5.825 GHz, with a sampling rate of 1000 packets per second. Widar3.0 mainly consists of two types of datasets. Firstly, there are 12,000 gesture samples commonly used in human-computer interaction (16 users \times 5 locations \times 5 orientations \times 6 gestures \times 5 instances). Secondly, there are 5,000 gesture samples representing digits 0-9 on a horizontal plane (2 users \times 5 locations \times 5 orientations \times 10 gestures \times 5 instances). To ensure a fair comparison, we only utilized 4,500 gesture samples (9 users \times 5 locations \times 5 orientations \times 6 gestures \times 5 instances) from the Widar3.0 dataset for source-free domain adaptation gesture recognition. The detailed descriptions of Widar3.0 dataset are provided in Tab. 4

Table 4: Detailed Descriptions of Widar3.0 Dataset

Environments	Users	Gestures	Locations	Orientations	Samples
1st (Classroom)	9	1: Push-Pull; 2: Sweep; 3: Clap; 4: Slide; 5: Draw-O(Horizontal); 6: Draw-Zigzag(Horizontal); 7: Draw-N(Horizontal); 8: Draw-Triangle(Horizontal); 9: Draw-Rectangle(Horizontal)	5	5	10,125
2nd (Hall)	4	1: Push-Pull; 2: Sweep; 3: Clap; 4: Slide; 5: Draw-O(Horizontal); 6: Draw-Zigzag(Horizontal)	5	5	3,000
3rd (Office)	4	1: Push-Pull; 2: Sweep; 3: Clap; 4: Slide; 5: Draw-O(Horizontal); 6: Draw-Zigzag(Horizontal)	5	5	3,000

Table 5: Detailed Descriptions of XRF55 Dataset

Environments	Users	Gestures	Locations	Orientations	Samples
Scene 1	30	1: Drawing circle; 2: Drawing cross; 3: Pushing; 4: Pulling; 5: Swiping left; 6: Swiping right; 7: Swiping up; 8: Swiping down	Changeable	Changeable	4,800
Scene 2	3	1: Drawing circle; 2: Drawing cross; 3: Pushing; 4: Pulling; 5: Swiping left; 6: Swiping right; 7: Swiping up; 8: Swiping down	Changeable	Changeable	480
Scene 3	3	1: Drawing circle; 2: Drawing cross; 3: Pushing; 4: Pulling; 5: Swiping left; 6: Swiping right; 7: Swiping up; 8: Swiping down	Changeable	Changeable	480
Scene 4	3	1: Drawing circle; 2: Drawing cross; 3: Pushing; 4: Pulling; 5: Swiping left; 6: Swiping right; 7: Swiping up; 8: Swiping down	Changeable	Changeable	480

XRF55 [56] is a large multi-radio frequency dataset for human action analysis, consisting of 42.9K samples of 55 action categories related to human-computer interaction collected from 39 users. To verify the effectiveness of the proposed Wi-CBR, we selected only the samples related to gesture actions collected using WiFi devices (e.g., drawing a circle, drawing a cross, pushing, pulling, swiping left, swiping right, swiping up, and swiping down) for the experiments. Among them, 30 users in environment 1 repeated the gestures 20 times within 5 seconds, and the remaining 9 users repeated the gestures 20 times within 5 seconds in the other three environments, totaling 6,240 samples. The detailed descriptions of XRF55 dataset are provided in Tab. 5

B Additional Experiments

Tab. 6 shows that Wi-CBR is comparable to the state-of-the-art competitors within the domain and much ahead in the cross-domain scenarios. Wi-CBR achieves the best results within the domain and in various cross-domain scenarios, even across different datasets. The reason for this is that hand-crafted features are very clever. Still, they may not be able to cover all the domain-independent sequential correlations scattered across the spatio-temporal dimension. For example, the BVP feature is cleverly designed but ignores which cues are essential and which are not. Therefore, we introduce phase and frequency domain data DFS guides containing all the information to capture the spatio-temporal cues in each modality. We also optimize the combined features for cross-fusion to obtain a robust domain-independent characterization.

Table 6: THE accuracy of Wi-CBR under In-Domain, Cross-location, Cross-orientation, and Cross-environment settings in the WIDAR3.0 dataset.

Methods	In-Domain	CL	CO	CE
Widar3.0 [7]	92.70%	89.70%	82.60%	92.40%
WiHF with HuFuM [8]	93.92%	90.32%	79.14%	89.67%
WiHF with HuFu [8]	97.65%	92.07%	82.38%	-
EI [49]	97.40%	73.33%	79.70%	-
WiGRUNT [37]	99.60%	96.49%	93.36%	93.73%
Wi-CBR	99.54%	98.34%	96.30%	96.57%

We evaluate Wi-CBR performance with different users(the default number is 9). The evaluation results are shown in Tab. 7. As the number of users increases, it can be observed that Wi-CBR has an upward trend, and the performance is higher for 9 types of users than for 6 types. This indicates that Wi-CBR can adapt to new users, while we observe that the overall trend of WiGRUNT is decreasing. The performance decreases significantly when the first user is added. We compare the effect of increasing the number of users on the system’s performance with WiGRUNT, and the results are shown in Fig. 5(a), which indicates that Wi-CBR is positively affected by the increase in the number of users.

Table 7: Comparison of Wi-CBR and WiGRUNT performance for different users.

No. of Users	Wi-CBR				WiGRUNT			
	6	7	8	9	6	7	8	9
In-Domain	99.07%	99.54%	99.63%	99.54%	99.60%	99.45%	99.48%	99.10%
CL	97.20%	98.46%	98.92%	98.34%	96.49%	96.21%	96.72%	96.17%
CO	95.31%	96.84%	97.08%	96.57%	93.36%	92.86%	94.11%	93.95%

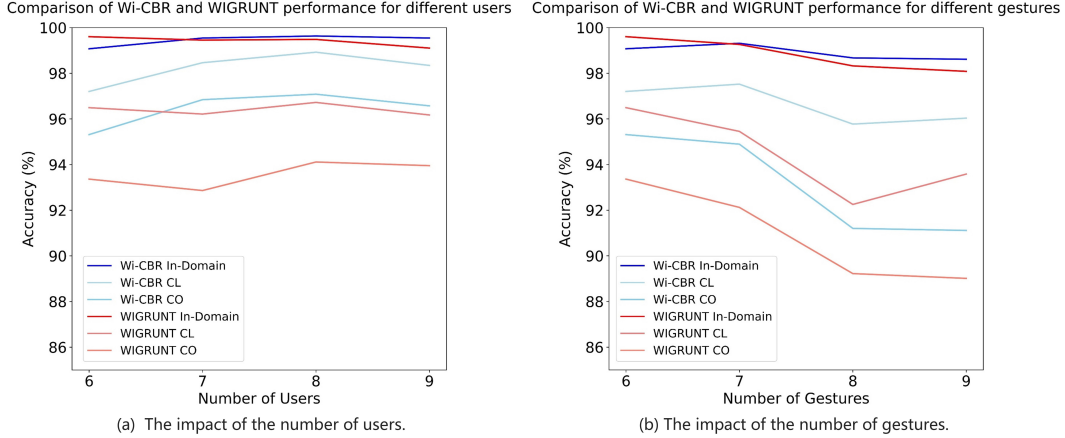


Figure 5: Overall comparison of users and gestures.

We evaluate Wi-CBR performance with different users(the default number is 6). The evaluation results are shown in Tab. 8. Unlike the effect of increasing users, a decreasing trend in performance

can be observed for both Wi-CBR and WiGRUNT as the number of gestures increases. However, for intra-domain and cross-location, Wi-CBR decreases slower than WiGRUNT and rises when encountering easily recognizable gestures. For cross-orientation, the two show parallel trends. WiGRUNT continues to decrease throughout, and the results are shown in the Fig. 5(b), which suggests that Wi-CBR’s performance feats are more stable as the number of gestures increases.

Table 8: Comparison of Wi-CBR and WiGRUNT performance for different gestures.

No. of Gestures	Wi-CBR				WiGRUNT			
	6	7	8	9	6	7	8	9
In-Domain	99.07%	99.31%	98.67%	98.61%	99.60%	99.26%	98.32%	98.08%
CL	97.20%	97.52%	95.77%	96.03%	96.49%	95.45%	92.25%	93.58%
CO	95.31%	94.89%	91.20%	91.11%	93.36%	92.12%	89.22%	89.01%

We plot cross-domain comparison histograms between Wi-CBR and state-of-the-art methods on the two datasets. The results are shown in Fig. 6, where Wi-CBR leads all previous methods that use unimodal data processing. Our two-branch extraction of spatio-temporal cues module ensures the effective utilization of phase and DFS data. At the same time, cross-modal cross-fusion yields unprecedentedly powerful domain-independent features. A significant advantage is achieved against model-based methods while outperforming the state-of-the-art method Wi-CBR by 8% under the XRF55 dataset.

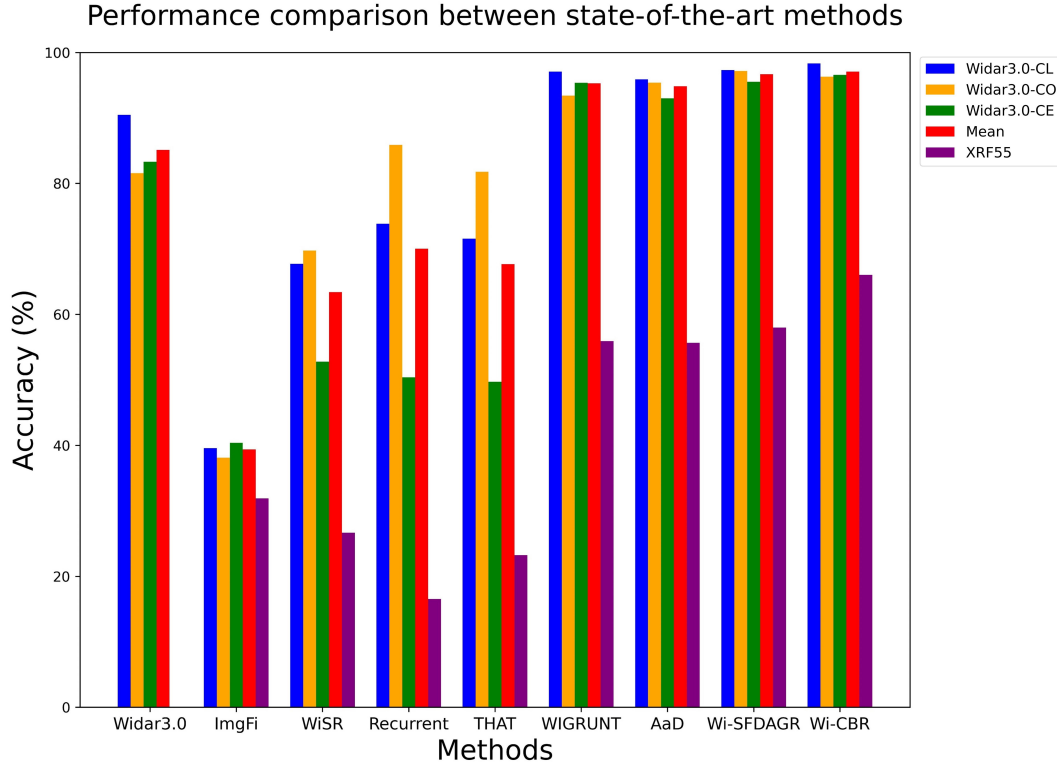


Figure 6: THE accuracy of Wi-CBR under CL(Cross-location), CO(Cross-orientation), and CE(Cross-environment) settings in the WIDAR3.0 dataset and the XRF55 dataset.